Tapio *et al. EURASIP Journal on Wireless Communications and Networking* (2020) 2020:127
https://doi.org/10.1186/s13638-020-01743-z

EURASIP Journal on Wireless Communications and Networking

RESEARCH Open Access

Self-interference cancelation in the presence of non-linear power amplifier and receiver IQ imbalance

Visa Tapio[1*], Marko Sonkki[1,2] and Markku Juntti[1]

*Correspondence: visa.tapio@oulu.fi
[1]Centre for Wirless Communications, University of Oulu, Oulu, Finland
Full list of author information is available at the end of the article

Abstract

In the in-band full-duplex(FD) systems, the self-interference (SI) power can be more than 100 dB higher than the power of the received data signal. In order to enable the FD transmission, several SI cancelation stages are needed in a FD transceiver. By combining the cancelation at the radio frequency (RF) with a specially designed antenna and cancelation circuitry and SI cancelation at the digital baseband, the required level of SI cancelation can be achieved even with a non-linear power amplifier. In this paper, a FD transceiver architecture is modeled with simulation tools that allow to use realistic antenna and analog transceiver models and at the same time enable algorithm studies. The analog SI cancelation at the RF is controlled by the baseband digital processing unit, and the tuning of the RF canceler is performed with an automatic gain control enhanced iterative algorithm. The combined cancelation performance of the antenna and RF canceler varies between 62 and 82 dB depending on the studied cases. The digital baseband SI cancelation is based on the Hammerstein model in order to take the power amplifier non-linearity into account. The coefficients of the Hammerstein model are estimated with a self-orthogonalizing adaptive algorithm. When realistic phase noise and IQ imbalance values are taken into account, the SI after all the cancelation stages can decrease the signal-to-interference-and-noise-ratio (SINR) by few decibels (dB). In order to further enhance the SI cancelation, the Hammerstein based SI canceler is extended to cancel also the effect of the receiver IQ imbalance. With the extended baseband canceler, the cancelation performance is mainly limited by the phase noise

Keywords: Full-duplex, Self-interference cancelation, Non-linearity, IQ imbalance

1 Introduction

In the in-band full-duplex (FD) transmission, the same carrier frequency is simultaneously used to transmit and receive data signals with the same transceiver. This offers the potential to double the system capacity when compared to a half-duplex (HD) system. An early attempt to realize the FD transmission was described in a 1949 patent [5] and discussed in [33]. Due to implementation challenges, the FD concept was considered infeasible for a long time. The drivers for the newborn interest for FD are the development in component and signal processing technologies as well as the emergence of short

range radio communication systems such as femto and other small-cell networks where the transmit powers can be much lower than in, e.g., mobile cellular systems with large cell sizes. Among the first realistic FD implementation concepts were the works introduced in [2, 12, 13].

The main problem of the FD systems is the self-interference (SI), i.e., the leakage of the transmit signal to the device's own receiver. Depending on the system, the SI cancelation requirement can be well over 100 dB. In order to achieve such high isolation values, several techniques for SI cancelation can be utilized in a FD transceiver. These include the antenna design, cancelation at radio frequency (RF), and cancelation at digital baseband [29]. The SI channel, i.e., the signal path from the transmitter to the receiver, includes reflections from the environment. Due to the movement of the transceiver or reflecting objects, the SI channel can be time-varying requiring the RF SI canceler to be tunable. The SI channel seen by the digital baseband processing unit is also time-varying and must be estimated for the digital SI cancelation.

The basic forms of active SI cancelation at RF and digital cancelation at the baseband were introduced in [12]. These principles have then been used in several published designs and are utilized also in this work. Other methods proposed for SI cancelation can be found, e.g., in [4, 10, 34].

In this paper, three different SI cancelation techniques are used in a single FD transceiver architecture. The antenna is designed using the characteristic modes theory. Additional attenuation at the RF processing is achieved by using the tunable active cancelation circuitry. The remaining SI after the analog cancelation is subsequently canceled at the digital processing. The digital cancelation is based on the Hammerstein model, which is used also in [1, 15, 18]. The usage of the Hammerstein model allows one to estimate the effect of non-linear power amplifier (PA) with linear estimation methods. The non-linearity model and linear filter used in the Hammerstein model results in large numbers of estimated parameters. In order to decrease the computational complexity, iterative algorithms have been used in the estimation of the Hammerstein model's parameters. As was noted in [18], the data used for the estimation is highly correlated. In [18], the decorrelation of the data has been done through the eigenvalue decomposition, which effectively implements the Karhunen-Loève transform. Another form of self-orthogonalizing adaptive filter was applied to acoustic echo cancelation in [19]. We extend it to the non-linear SI cancelation. The Hammerstein model-based SI canceler is not able to take into account the distortion caused by the gain and phase mismatches of the in-phase (I) and quadrature (Q) signal paths of a transceiver called IQ imbalance. The estimation of the IQ imbalance parameters for SI cancelation has been considered in [16, 17]. In this paper, the self-orthogonalizing adaptive filter is further extended to jointly estimate the effect of the PA non-linearity and receiver IQ imbalance when the data used for the estimation is correlated. This paper summarizes and extends the work by the authors published earlier. The joint compensation of the IQ imbalance and power amplifier non-linearity in SI cancelation with the used method has not been published previously.

The rest of the paper is organized as follows. The research method and main contributions are described in Section 2. The system model and transceiver architecture are described in Section 3, the SI channel model is described in Section 4, the SI cancelation

methods are described in Section 5, and link capacity of a FD link is discussed in Section 6. Numerical results are given in Section 7, and finally, conclusions are presented in Section 8.

2 Research method

The research method in this paper is based on the co-simulation of analog transceiver and digital signal processing. This approach allows to study the interworking of the digital signal processing and analog transceiver as well as to model the control of the analog parts of the transceiver with the digital processing unit. Further, the tools used allow to incorporate realistic models for the analog parts and also to use the component parameters from data sheets of the commercial components. The selected approach does not replace the importance of prototype building, but it allows efficient ways to test different implementation architectures and enables to assess individually the effect of different non-ideal behaviors, such as non-linearity, IQ imbalance, and phase noise.

The main contributions are the evaluation of the combined performance of an antenna and RF canceler with realistic component models, the application and performance evaluation of the self-orthogonalizing adaptive filter in the digital baseband SI cancelation, and the assessment of the effects of the performance of the combined RF and digital cancelation on the link capacity when the link is capable to switch between the HD and FD modes. The performance of the RF canceler includes the convergence rate and total isolation of the antenna and the SI cancelation circuitry operating at RF. The inclusion of the analog-to-digital (A/D) converter models into the transceiver model necessitates the control of the input power of the A/D-converters in order to prevent the overloading of the converters and at the same time utilize the full dynamic range of them. This is done by combining the tuning of the RF canceler with the automatic gain control (AGC). In digital SI cancelation, the linear part and non-linear distortion of the SI signal as well as the distortion caused by the IQ imbalance at the receiver are attenuated. The effect of the remaining IQ imbalance and phase noise on the baseband cancelation and FD link performance is also evaluated.

3 System model and transceiver architecture

The system model is shown in Fig. 1. Node 1 is a FD transceiver capable of simultaneously transmitting and receiving at the same carrier frequency. If it is communicating with node 2, the system is a FD link between two FD transceivers, i.e., node 2 is also able to operate in the FD mode. This system is drawn with solid lines. The second option is indicated by the dashed lines. Therein, node 1 receives a signal from node 2 and at the same time using the same carrier frequency transmits to node 3. In this option, only node 1 needs to be a FD transmitter; the other nodes can operate in the HD mode. The second option includes the case of relaying a message from node 2 to node 3 or node 1 can be serving an up- and down link user simultaneously. From the SI cancelation point of view at node 1, all these cases are similar.

A block diagram of a full duplex transceiver is shown in Fig. 2. The two multipliers in Fig. 2 represent the up- and down-converting mixers. The local oscillators (LO) needed in the frequency conversions are not drawn to the transceiver model. The LPF blocks are low pass filters. The LPF at the transmitter is used to suppress the power at the adjacent

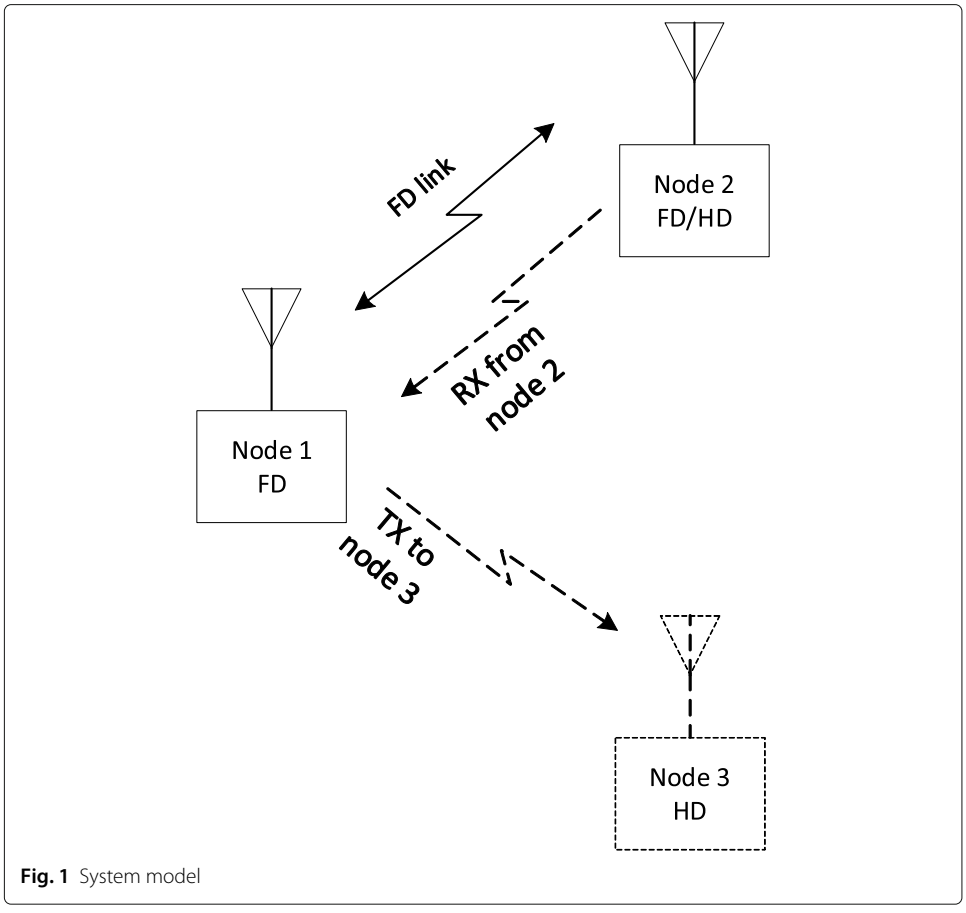

Fig. 1 System model

channels. The LPF at the receiver is used to select the received data signal from the down-converted signal band. The D/A and A/D blocks are the digital-to-analog and analog-to-digital converters at the transmitter and receiver, respectively. The PA block stands for power amplifier and LNA is the low noise amplifier at the receiver. The arrow on the amplifier G_{BB} means that its gain is controllable by the automatic gain control (AGC).

4 Self-interference channel model

The SI channel consists of the leakage through the antenna and the reflections from the operating environment of a FD transceiver. Although there are some published measurements of a SI channel [23, 32], there are no widely accepted models for the SI channel.

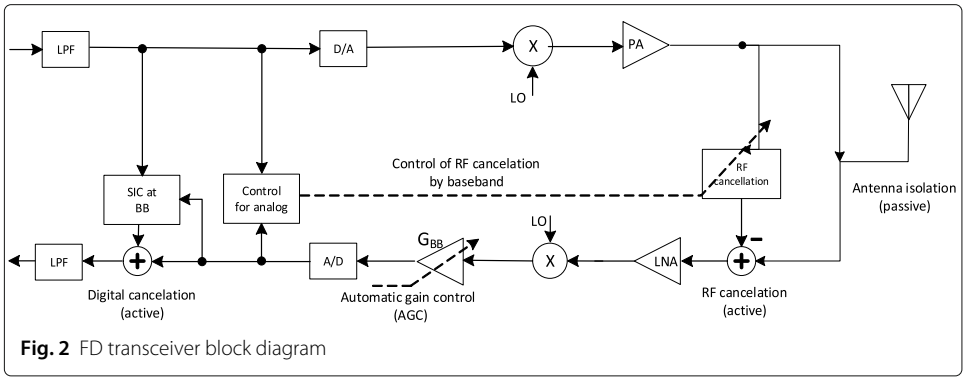

Fig. 2 FD transceiver block diagram

A SI channel modeling approach proposed in [29] is used here. The channel tap gains are calculated based on the assumed distances of the reflecting surfaces and reflection coefficients of typical construction materials. The attenuation of a reflection path i is

$$L_i = L^i_{\text{free}} + L^i_{\text{R}} - G^i_{\text{tx}} - G^i_{\text{rx}}, \tag{1}$$

where L^i_{free} is the free space loss of the ith path

$$L^i_{\text{free}} = 20\log_{10}(2d_i) + 20\log_{10} f + \log_{10}\frac{4\pi}{c}, \tag{2}$$

d_i is the distance in meters between the transceiver and reflecting surface, f is the frequency in hertz, and c is the speed of electromagnetic radiation. The loss component caused by the reflection is

$$L_{R_i} = 20\log_{10} R_i, \tag{3}$$

where the reflection coefficient R_i is [7, 24]

$$R_i = \frac{\sin\theta_i - Z_i}{\sin\theta_i + Z_i}, \tag{4}$$

and [7], [24]

$$Z_i = \begin{cases} \sqrt{\frac{1}{\varepsilon^2_{r_i}}(1-\cos\theta_i)} & \text{(vertical polarization)} \\ \sqrt{\epsilon_{r_i} - \cos^2\theta_i} & \text{(horizontal polarization).} \end{cases} \tag{5}$$

ε_{r_i} is the relative permittivity of the ith reflecting surface and θ_i is the grazing angle of ith reflection. G^i_{tx} and G^i_{rx} in (1) are the gains of the antenna in the transmit and reception direction of the reflections. Since the ith reflection path is assumed to include only one reflection, i.e., the reflected signal is received from the same direction where it was radiated, antenna gains are equal. The ray tracing approach can also be extended to include multiple reflections in a single multipath component.

5 SI cancelation

The SI cancelation can be done using several different techniques. Since the cancelation requirement can be well over 100 dB, a FD transceiver needs to utilize more than one of those techniques. Typically, the first SI attenuation is achieved by the antenna and an additional circuitry is used to provide additional cancelation at RF. After the down-conversion and A/D-conversion, the SI can be further attenuated by signal processing. It is also possible to perform SI cancelation at analog baseband before the A/D-conversion, but if the SI signal contains several delayed components (multi-tap SI channel), an accurate delay estimate is needed for the analog baseband cancelation.

Three different techniques for the SI cancelation are included in the architecture in Fig. 2: isolation provided by the antenna, SI cancelation at RF, and digital SI cancelation. Antenna design is based on the theory of characteristic modes (TCM)[6, 8]. With TCM, a conducting body can be studied in terms of orthogonal radiating modes which are naturally isolated. This can be also seen as a set of two dipole antennas oriented in orthogonal polarization. Thus, two orthogonal modes give a good solution for the FD transceiver with high antenna isolation between transmit and receive antenna ports. The used planar antenna model is described in [25]. The operation frequency of the antenna in [25] is different from the frequency used in this paper but the operation principle is the same. The same antenna design was used also in [26, 27, 29, 30]. The RF canceler is shown in Fig. 3.

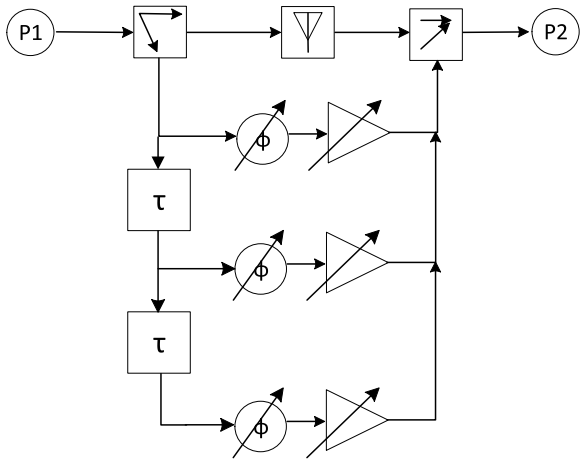

Fig. 3 Antenna and RF SI cancelation

It consists of an FIR filter type structure where the phase (ϕ) and gain values of each tap can be tuned. The delay (τ) equals the sample time of the A/D converters. The tuning of the RF canceler is controlled by the digital baseband processing unit as indicated by the dashed line in Fig. 2. For the digital SI cancelation, the SI channel is first estimated and the estimate is then used to generate an estimate of the SI signal. The SI channel estimated at the receiver includes the transmit chain, antenna and reflections from the environment and the receiver chain. The SI cancelation is performed by subtracting the estimate of the SI signal from the signal at the output of the A/D converters.

5.1 Control of the RF canceler

Since changes in the environment cause the SI channel to change, the SI canceler must be tunable. The tuning of the RF canceler is done with a transmitted data signal in a half duplex mode, i.e, no FD specific training signals for the tuning are needed. A gradient algorithm is used for the tuning. At each iteration step, a complex coefficient vector $\mathbf{w}(k)$ is calculated as

$$\mathbf{w}(k) = \mathbf{w}(k-1) - \frac{\mu_i}{MP_{\mathrm{x}}} \sum_{n=1}^{M} y_{\mathrm{rx}}(n)\mathbf{x}_{\mathrm{SI}}^{*}(n), \tag{6}$$

where k is the iteration index, M is the number of samples per iteration, P_{x} is the power of the SI signal x_{SI}, y_{rx} is the received signal, and μ_i is the step size of the algorithm. The numerical values of μ_i depend on the properties of the signal as well as on the properties of the transceiver, especially the gain of the receiver, and they have been selected by simulations to allow fast convergence at the beginning and good accuracy at the end of the tuning. Vector $\mathbf{x}_{\mathrm{SI}}$ consists of samples $x_{\mathrm{SI}}(n), x_{\mathrm{SI}}(n-1)\cdots x_{\mathrm{SI}}(n-N)$ for an N length SI canceler. The gains of the amplifiers and phase values for the phase shifters in Fig. 3 are calculated as the absolute values and phases of the elements of the vector $\mathbf{w}$, respectively.

During the tuning, the signal levels at the inputs of the A/D converters are reduced. In order to utilize the full dynamic range of the A/D converters during the tuning, AGC is used to control the level of the A/D converters' input signals by controlling the gain of the amplifier G_{BB} in Fig. 2 using Algorithm 1

Algorithm 1: Automatic gain control (AGC)

if $P_{rx} > P_{th}$ **then**
  $G_{\mathrm{BB}}(k) = G_{\mathrm{BB}}(k-1) - \Delta G_{\mathrm{BB}}$
else if $P_{BB}(k) < P_{BB}(k-1) - 3\ dB$ ***and*** $G_{RF} < G_{RF,max}$ **then**
  $G_{\mathrm{BB}}(k) = G_{\mathrm{BB}}(k-1) + \Delta G_{\mathrm{BB}}$
end

where P_{th} is a threshold power for preventing ADC overload and ΔG_{BB} is the change in the gain measured in decibels (dB). Algorithm 1 keeps the input powers of the A/D-converters inside the upper half of their dynamic ranges. In simulations of Section 7.2, the ΔG_{BB} is set to 2 dB.

In order to increase the convergence rate further, the variable step size μ_i in (6) is also chosen based on the gain of the G_{BB} [27].

5.2 Digital baseband cancelation with PA non-linearity compensation

After the tuning of the RF canceler has stopped, the SI channel estimation at the baseband can be performed. The channel estimate needs to include also the effect of non-ideal operation of the transceiver. It is assumed that the PA is the dominating non-linear component in the system and the impact of other nonlinearities can be ignored. The transmitter chain before the PA is further assumed to have a flat frequency response, i.e., it can be modeled as a 1-tap channel. In this case, the combination of the transceiver and the channel between the PA and LNA can be modeled as a Hammerstein system. The PA is assumed to be a memoryless non-linear amplifier and its output is modeled as a baseband polynomial function [35]

$$\begin{aligned} x_1(n) &= \sum_{q=0}^{Q} a_{2q+1} u_1(n) |u_1(n)|^{2q} \\ &= \sum_{q=0}^{Q} a_{2q+1} u_1(n)^{q+1} [\, u_1^*(n)]^q \,, \end{aligned} \tag{7}$$

where $u_1(n)$ is the transmitted baseband signal before the D/A converter in Fig. 2, coefficients a_{2q+1} are used to characterize the non-linearity and Q is the order of the non-linearity.

The linear SI channel after the PA consists of the direct leakage path through the antenna, reflection paths in the environment, and the receiver chain, which is assumed to be linear. For the SI cancelation, the linear path of the channel is modeled as a linear FIR filter. The output of the filter is

$$\begin{aligned} u_2(n) &= \sum_{d=0}^{D-1} \sum_{q=0}^{Q} h(d) x_1(n-d) \\ &= \sum_{d=0}^{D-1} \sum_{q=0}^{Q} h(d) a_{2q+1} u_1(n-d) |u_1(n-d)|^{2q}, \end{aligned} \tag{8}$$

where $h(d)$ are the coefficients of the SI channel and D is the length of the channel.

In system modeling, the goal is generally the estimation of both the h and a_{2q+1} in (8). However, in SI cancelation, the separation of the parameters is not necessary, hence (8) can be written as

$$u_2(n) = \sum_{d=0}^{D-1} \sum_{q=0}^{Q} w_{d,q} u_1(n-d)|u_1(n-d)|^{2q}, \tag{9}$$

which can be written in matrix format as

$$\mathbf{u}_2 = \mathbf{U}\mathbf{w}, \tag{10}$$

where $\mathbf{u}_2 = [\, u_2(n) \ \cdots \ u_2(n+D)]$, vector $\mathbf{w} = [\, w_{0,0} \ \cdots \ w_{D-1,Q}]^{\mathrm{T}}$ contains the unknown coefficients and matrix $\mathbf{U}$ for the third order non-linearity ($Q = 1$) is

$$\mathbf{U} = \begin{bmatrix} u_1(n) & \cdots & u_1(n-D) & u_3(n) & \cdots & u_3(n-D) \\ u_1(n+1) & \cdots & u_1(n-D+1) & u_3(n+1) & \cdots & u_3(n-D+1) \\ \vdots & \vdots & \vdots & \vdots & \vdots & \vdots \\ u_1(n+D) & \cdots & u_1(n) & u_3(n+D) & \cdots & u_3(n) \end{bmatrix} \tag{11}$$

and $u_3(n) = u_1(n)|u_1(n)|^2$. The estimate of the filter coefficient vector $\mathbf{w}$ can be computed with a self-orthogonalizing adaptive filtering algorithm [9, 19, 22]. The filter coefficient vector is calculated iteratively as

$$\widehat{\mathbf{w}}(k+1) = \widehat{\mathbf{w}}(k) + \mu_d \mathbf{C}_u^{-1} \nabla_{u_1}, \tag{12}$$

where $\mathbf{C}_u$ is the covariance matrix of the transmitted signal, the gradient vector is

$$\begin{aligned} \nabla_{u_1} = [\, & u_1^*(n) \ \cdots \ u_1^*(n-D) \\ & u_1^*(n)|u_1(n)|^2 \ \cdots \ u_1^*(n-D)|u_1(n-D)|^2]^{\mathrm{T}}. \end{aligned} \tag{13}$$

and μ_d is the step-size of the algorithm. The upper bound for the step size to guarantee the convergence is [3]

$$\mu_d < 2 \cdot D \cdot P_x \tag{14}$$

where P_x is the power of the complex baseband signal after the A/D-conversion. In the simulations reported in Section 7.3, the step size has been $\mu_d = 2P_x$.

The covariance matrix of the transmitted data does not vary during the transmission as long as the modulation method and the signal bandwidth do not change; hence, it and its inverse can be calculated off-line and saved to the memory of the FD transceiver. When calculating the covariance matrix, the non-linearity model must be taken into account. The estimate of the covariance matrix is calculated as

$$\mathbf{C}_u = \frac{1}{N_{\mathrm{c}}} \sum_{j=0}^{N_{\mathrm{c}}-1} \mathbf{u}(j)\mathbf{u}^{\mathrm{H}}(j), \tag{15}$$

where

$$\begin{aligned} \mathbf{u}(j) = [\, & u_1(j) \ \cdots \ u_1(j-D) \\ & u(j)|u_1(j)|^2 \ \cdots \ u_1(j-D)|u_1(j-D)|^2]^{\mathrm{T}} \end{aligned} \tag{16}$$

and N_{c} is the number of samples used to calculate $\mathbf{C}_u$.

After the coefficient vector $\mathbf{w}$ has been estimated, the baseband SI cancelation is performed by subtracting $u_2(n)$ from the output signal of the A/D-converter in Fig. 2

5.3 Baseband cancelation with the compensation of power amplifier non-linearity and receiver IQ imbalance

In addition to the PA non-linearity, there are other non-ideal characteristics of a transceiver that affect the SI cancelation performance. One of these is the IQ imbalance. The IQ imbalance can be modeled as [31]

$$y_{IQ} = \mu_{\mathrm{RX}} x_{\mathrm{IQ}} + \nu_{\mathrm{RX}} x^*_{\mathrm{IQ}}, \tag{17}$$

where x_{IQ} and y_{IQ} are the signals before and after the IQ imbalance. The parameters μ_{RX} and ν_{RX} are defined using the amplitude imbalance (ξ) and phase imbalance (θ) as

$$\begin{aligned} \mu_{\mathrm{RX}} &= \cos(\theta/2) + j\xi \sin(\theta/2) \\ \nu_{\mathrm{RX}} &= \xi \cos(\theta/2) - j \sin(\theta/2). \end{aligned} \tag{18}$$

Using the IQ imbalance model (17) and the Hammerstein non-linearity model (9), the combined effect of the PA non-linearity and receiver IQ imbalance is modeled as

$$\begin{aligned} u_2(n) =& \mu_{\mathrm{RX}} \sum_{d=0}^{D-1} \sum_{q=0}^{Q} w_{d,q} u_1(n-d)|u_1(n-d)|^{2q} + \\ & \nu_{\mathrm{RX}} \sum_{d=0}^{D-1} \sum_{q=0}^{Q} w^*_{d,q} u^*_1(n-d)|u_1(n-d)|^{2q}, \end{aligned} \tag{19}$$

For the SI cancelation, the separation of the parameters is not needed as explained in Section 5.2; the IQ model parameters and the coefficients of the non-linearity model can be combined. Hence, the effect of the non-linear PA and IQ imbalance can be written as

$$\begin{aligned} u_2(n) =& \sum_{d=0}^{D-1} \sum_{q=0}^{Q} \tilde{w}_{d,q} u_1(n-d)|u_1(n-d)|^{2q} + \\ & \sum_{d=0}^{D-1} \sum_{q=0}^{Q} \breve{w}_{d,q} u^*_1(n-d)|u_1(n-d)|^{2q}. \end{aligned} \tag{20}$$

The estimation of the parameter vectors $\tilde{\mathbf{w}}$ and $\breve{\mathbf{w}}$ is done in two phases. In the first phase, the second term in (20) is considered to be part of the noise in the received signal and the SI cancelation is performed as in Section 5.2. After the first phase, the coefficient vector $\breve{\mathbf{w}}$ is estimated iteratively from the residual SI still present in the output signal of the SI canceler as

$$\widehat{\breve{\mathbf{w}}}(k+1) = \widehat{\breve{\mathbf{w}}}(k) + \mu_d \mathbf{C}_u^{-1} \nabla^*_{u_1}, \tag{21}$$

where $\nabla^*_{u_1}$ is the complex conjugate of the gradient vector (13). After the coefficient vectors have been estimated, the SI cancelation is performed as

$$\begin{aligned} y_{\mathrm{SI}}(n) =& x_{\mathrm{SI}}(n) - \sum_{d=0}^{D-1} \sum_{q=0}^{Q} \hat{\tilde{w}}_{d,q} u_1(n-d)|u_1(n-d)|^{2q} \\ & - \sum_{d=0}^{D-1} \sum_{q=0}^{Q} \hat{\breve{w}}_{d,q} u^*_1(n-d)|u_1(n-d)|^{2q}, \end{aligned} \tag{22}$$

where $x_{\mathrm{SI}}(n)$ is the signal before digital baseband SI cancelation.

6 Effect of SI cancelation performance on the FD link sum rate

The performances of the analog and digital SI cancelation methods affect the link sum rate via the residual SI power after all the cancelation steps and resources needed by the cancelers.

The maximum achievable sum rate of a HD link in white Gaussian noise channel (AWGN) is

$$R_{HD} = \alpha(1-\kappa_{HD,1})\log_2(1+\gamma_1) + (1-\alpha)(1-\kappa_{HD,2})\log_2(1+\gamma_2), \tag{23}$$

where α defines the proportion of transmission times of nodes 1 and 2 (see Fig. 4), $\kappa_{HD,1}$ and $\kappa_{HD,2}$ are the pilot overheads of the received signals in the HD link, and γ_1, γ_2 are the receive signal-to-interference-plus-noise ratios (SINR) at nodes 1 and 2, respectively. If the SINR is the same at both nodes ($\gamma = \gamma_1 = \gamma_2$) and the pilot overhead in both directions is the same ($\kappa_{HD,1} = \kappa_{HD,2} = \kappa_{HD}$), (23) reduces to

$$R_{HD} = (1-\kappa_{HD})\log_2(1+\gamma) \tag{24}$$

When the nodes are operating in the FD mode, the link capacity is affected by the residual SI after the cancelation, the pilot overhead needed for the SI cancelation at the digital baseband, and the time needed to tune the RF canceler and estimate the SI channel. If the RF canceler is not tuned correctly, the SI at the receiver can overload the receiver unless AGC is not used to control the signal power at the input of the A/D converters preventing the reception of a data signal from a distant node. Even when the AGC is used, the received signal can be blocked by the SI and the increased noise level at the receiver. Hence, it is assumed that during the tuning of the RF canceler, the node cannot decode the data. The tuning of the RF canceler as well as the baseband SI channel estimation can be performed using a training signal or in the HD mode using the transmitted data signal.

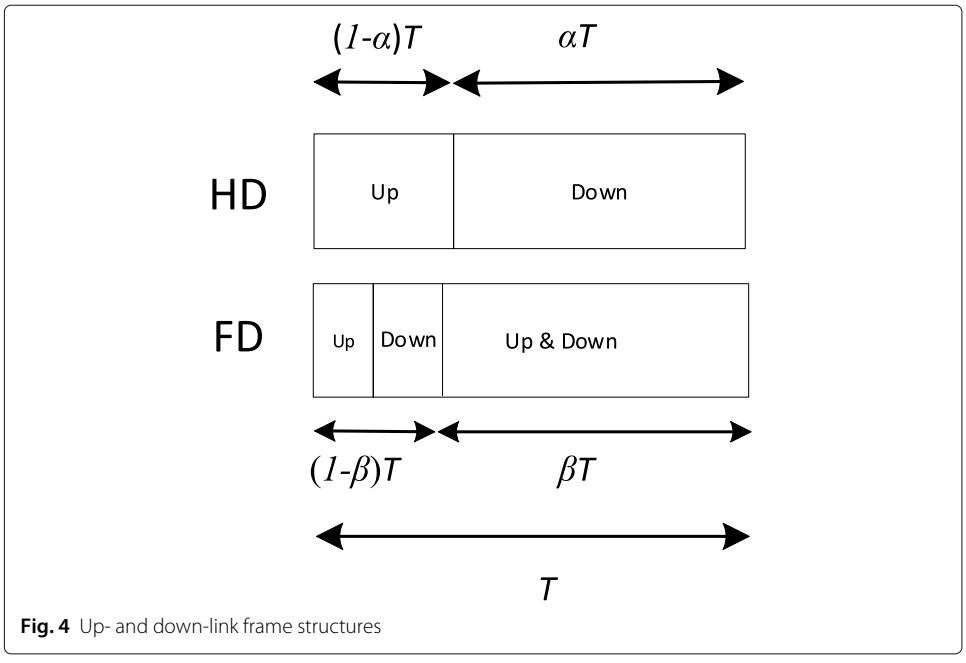

Fig. 4 Up- and down-link frame structures

After the tuning has stopped and the SI channel has been estimated, the link is switched to the FD mode. Parameter $\beta \in [0,1]$ defines the proportion of time spent in the HD and FD modes. If the HD mode requires the usage of additional FD specific pilots for SI channel estimation in digital baseband SI cancelation, the capacity is further reduced by the factor κ_{FD}. By taking into account of these factors, the sum rate of a FD link is

$$R_{FD} = \beta(1-\kappa_{FD}-\kappa_{HD})[\log_2(1+\gamma_1) + \log_2(1+\gamma_2)] + (1-\beta)R_{HD}. \tag{25}$$

If the tuning of the RF canceler is done with a training signal, i.e., no data is sent during the tuning, the last term in (25) is zero. SINR terms (γ_1, γ_2) include the thermal noise and residual SI after the SI cancelation.

7 Numerical results

7.1 Transceiver and signal model

The signal used in the simulations is an orthogonal frequency-division multiplexing (OFDM) signal with 48 data sub-carriers and 4 pilot sub-carriers at 3.5 GHz center frequency. Data sub-carriers are modulated using 16 level quadrature amplitude modulation (16-QAM). The bandwidth of the signal is 20 MHz. The antenna is modeled using an electromagnetic simulation tool (CST Microwave Studio). Simulated S-parameters are brought to the system model as an S-parameter file. The FD transceiver including the analog SI cancelers and A/D converters is modeled using the Advanced Design System (ADS). The maximum values of the integral (INL) and differential (DNL) non-linearity to least significant bit of the A/D converters are 5.0 and 0.7, respectively. The IQ imbalance and phase noise data is taken from [21]. The phase and amplitude imbalance of the transceivers are 0.5° and 0.1 dB, respectively. The phase noise is characterized with the values in Table 1. The PA is modeled using a non-linear amplifier model available in ADS. The amplifier non-linearity is characterized by the 1 dB compression point ($P_{1\text{dBc}}$) and the output's third-order intermodulation intercept point (TOI). The numerical values used in the simulations are 25 dBm and 35 dBm for $P_{1\text{dBc}}$ and TOI, respectively.

7.2 SI cancelation at RF

The performance of the RF canceler is shown in Fig. 5a. The *SI power attenuation* axis gives the amount of additional SI isolation in dB provided by the RF canceler. The total SI isolation at RF is then the sum of this additional isolation and isolation provided by the antenna. The *iteration index* axis is k in (6). At each iteration, the update in coefficient $\mathbf{w}$ is calculated using 1 OFDM symbol. With the used signal model this equals 4 μs. The SIC1 curve is from [30], and it represents the case when the SI channel consists of the

Table 1 Phase noise

Freq. offset	Phase noise
1 kHz	− 87 dBc
10 kHz	− 103 dBc
100 kHz	− 99 dBc
1 MHz	− 112 dBc
10 MHz	− 125 dBc

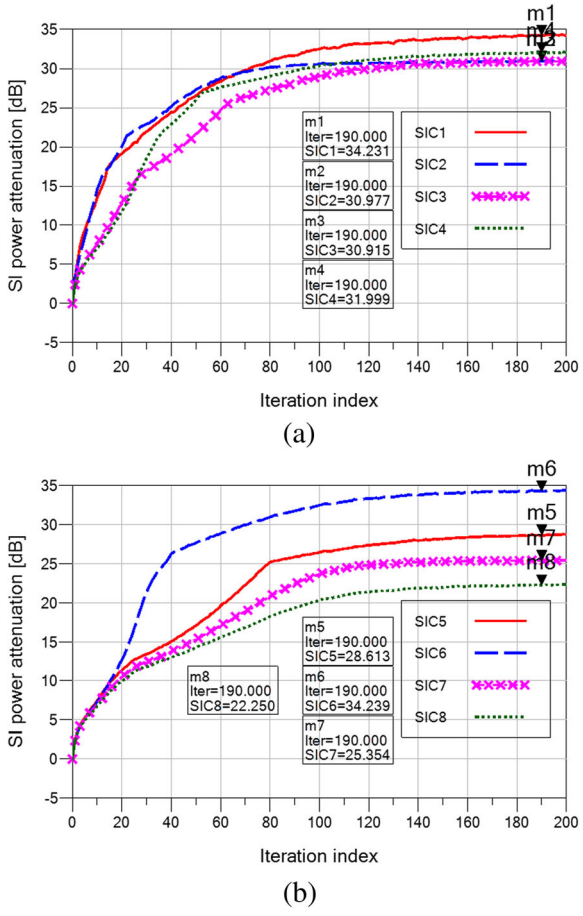

Fig. 5 Additional SI cancelation provided by the RF canceler when the antenna isolation without reflections is 61 dB: **a** SI channel delay smaller or equal to RF canceler delay, **b** SI channel delay longer than RF canceler delay

direct leakage through the antenna and three reflections from the environment at the distances of 0.5 m, 1 m, and 3 m. The delay attenuation pairs for the paths are (3.33 ns, 45 dB), (6.67 ns, 50 dB), and (20.0 ns, 55 dB). In this case, the number of reflections is the same as the number of taps in the RF canceler. The SIC2, SIC3, and SIC4 curves represent the cases when a fourth (2 m, 13.33 ns, 51 dB), fifth (0.75 m, 5.0 ns, 47 dB), and sixth (3.75 m, 25.0 ns, 56 dB) reflections have been added to the SI channel model, respectively. In all these cases, the delays of the paths have been shorter or equal to the maximum delay of the RF canceler (= 25 ns). In Fig. 5b, the SIC5, SIC6, SIC7, and SIC8 curves show the performance when the length and delay of the longest path have been increased to 4.5 m, 30 ns, 5.25 m, 35 ns, 6.0 m, 40 ns, and 7.5 m, 50 ns. The path loss of the longest path in these cases has been 57 dB.

When there are no reflections from the environment, the antenna provides 61 dB isolation over the signal bandwidth. The antenna cannot attenuate the reflected SI components; hence, the antenna isolation is reduced when there are reflections present. Table 2 gives the isolation values in dB for the antenna only case, the additional isolation provided by the RF canceler, and the total isolation. All the values in Table 2 are given in

Table 2 Isolation provided by the original antenna and the RF canceler and the total isolation in dB

	SIC1	SIC2	SIC3	SIC4	SIC5	SIC6	SIC7	SIC8
Antenna only	48.6	44.5	40.1	39.1	40.9	39.4	40.6	40.3
RF canceler	34.2	31.0	31.0	32.1	28.6	34.2	25.4	22.3
Total	82.8	75.5	71.1	71.2	69.5	73.6	66.0	62.6

dB. The isolation values for the RF canceler are taken from the marker positions (m25-32) in Fig. 5.

In Fig. 6, the reflections are the same as in the cases reported in Fig. 5 and Table 2 but antenna model has been modified from the original one. The shape of the frequency response of the antenna has not been altered, but the isolation in the case when there are no reflections has been reduced by 20 dB to 41 dB.

The results in Tables 2 and 3 indicate that when the numbers of reflections and taps in the RF canceler are the same, the higher antenna isolation (61 dB) gives a better performance than the antenna with lower isolation (41 dB). However, when the number of reflections increases, the total isolation is in the same order with both the antennas and in

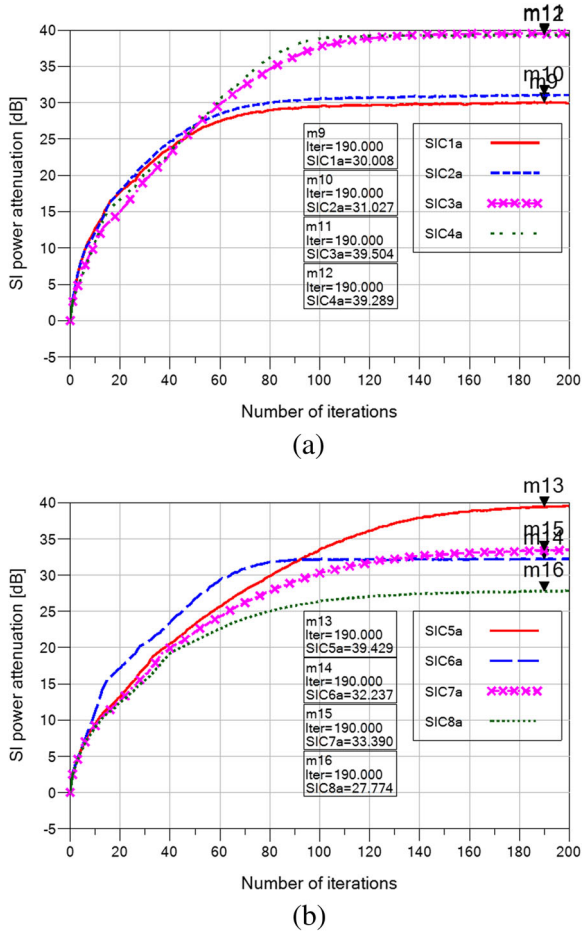

Fig. 6 Additional SI cancelation provided by the RF canceler when the antenna isolation without reflections is 41 dB: **a** SI channel delay smaller or equal to RF canceler delay, **b** SI channel delay longer than RF canceler delay

Table 3 Isolation provided by the modified antenna and the RF canceler and the total isolation in dB

	SIC1a	SIC2a	SIC3a	SIC4a	SIC5a	SIC6a	SIC7a	SIC8a
Antenna only	41.4	41.9	38.6	37.7	39.2	38.0	38.9	38.7
RF canceler	30.0	31.0	39.5	39.3	39.4	32.2	33.4	27.8
Total	71.4	72.9	78.1	77.0	78.6	70.2	72.3	66.5

some cases, the antenna with lower isolation combined with the RF canceler can give better SI cancelation performance than the combination of the RF canceler and the antenna with higher isolation. These results show that when the SI channel includes reflections from the environment, the increased antenna isolation does not necessarily improve the cancelation performance since the reflected SI is received by the antenna without attenuation. The variation of the cancelation performance in Tables 2 and 3 depends also on how different reflected SI components add at the receiver (constructively or destructively).

7.3 Digital baseband SI cancelation

After the RF canceler has been tuned, the SI channel is estimated at the baseband digital processing unit. The SI channel between the antenna input and output ports and the state of the RF canceler are from the case SIC1 in Fig. 5a. The performance of the digital SI canceler is measured by the increase in the noise level when compared to the HD case. The results in Fig. 7a and b show the increase in the noise level as a function of the transmitted power (SI power at the PA output). The *linear PA* curve shows the increase in the noise level with a linear PA. In this case, the SI channel is estimated with a least squares (LS) estimator. The *Non-linear PA, linear canc.* curve shows the performance with a non-linear PA when the SI channel is estimated with the same LS estimator as in the linear PA case. The *Non-linear PA, LMS canc.*, and *LMS canc with IQ comp.* curves give the performances of the estimators described in Sections 5.2 and 5.3, respectively. In these four cases, the phase noise and IQ imbalance at the transmitter and receiver are the same as those given in Section 7.1. As it can be seen from Fig. 7a, the noise enhancement in the linear PA case and non-linear PA with the Hammerstein model-based SI cancelation case are about the same. When the receiver IQ imbalance is taken into account, the residual interference after the cancelation is further reduced. This suggests that the effect of non-linear PA and receiver IQ imbalance can be efficiently compensated with the used methods and that the transmitter IQ imbalance and phase noise at the transmitter and receiver cause the performance degradation.

In order to separate the effect of the phase noise and IQ imbalance in the non-linear PA case, simulations in the case of phase noise only, IQ imbalance at the transmitter and receiver, IQ imbalance at receiver only, and IQ imbalance at transmitter only were performed. The SI cancelation is done as described in Section 5.2. The results of the simulations are given in Fig. 7b. When the transmit power is 20 dBm and there is no IQ imbalance at the transmitter nor the receiver, the phase noise increases the noise floor with about 0.8 dB. In the cases of IQ imbalance in the transmitter or receiver (no phase noise), the noise increase is about 1 dB. As can be seen from Fig. 7a, the residual SI at 20 dBm transmit power with the IQ imbalance compensation is 1 dB lower than without it. This shows that the proposed method efficiently cancels the combined effect of receiver IQ imbalance, PA, and the linear part of the SI channel.

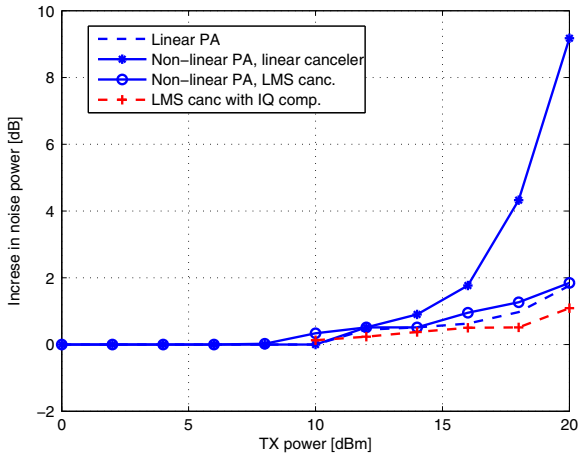

(a) Noise enhancement

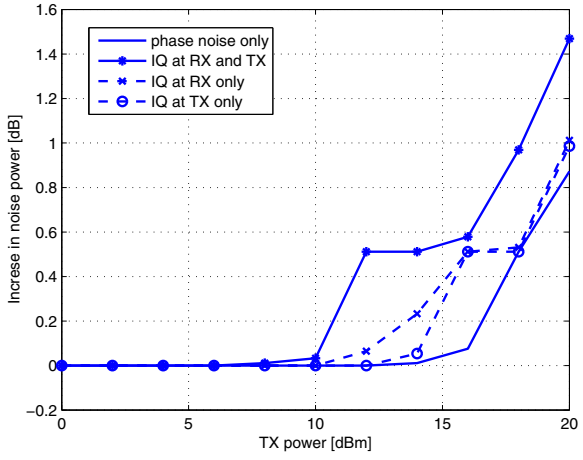

(b) Noise enhancement components

Fig. 7 Increase in noise level after digital SI cancelation. **a** Total noise enhancement. **b** Noise enhancement components

7.4 Bit error rate performance

The bit error rate (BER) simulations are run in the case represented by the column SIC1 in Table 2. After the SI channel has been estimated, the system switches to FD mode. It is assumed that the SI channel does not change during the FD transmission. The channel between node 1 and node 2 is an additive white Gaussian noise (AWGN) channel. The BER results are given in Fig. 8[1]. The *HD* curve shows the performance of a HD link. The *FD* 10 *dBm* and *FD* 20 *dBm* curves show the performance without IQ compensation when the transmit power has been 10 dBm and 20 dBm, respectively. The curves *FD* 10 *dBm, IQ comp*, and *FD* 20 *dBm, IQ comp* show the performance with IQ compensation. In all these five cases, the IQ imbalance and phase noise values are those listed in Section 7. The *FD, Ideal TxRx* 20 *dBm* curve shows the performance when the transmit power is 20 dBm and there is no phase noise or IQ imbalance in the transceiver. When the transmit power is 10 dBm or lower, the BER performance of the FD link is the same as that of the HD

[1]Roughness in the BER curves is due to the limited number of iterations in ADS/Matlab co-simulations.

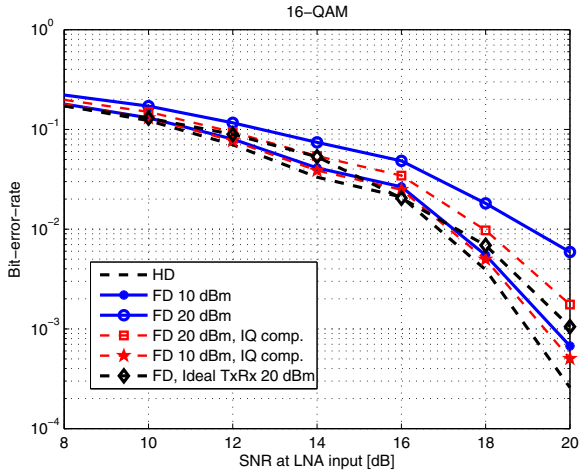

Fig. 8 BER vs. SNR in AWGN channel

link. When the transmit power is increased to 20 dBm, the BER performance without IQ compensation is about 2 dB worse and with IQ compensation about 1 dB worse than the performance of an ideal FD receiver as is expected based on the results in Section 7.3.

The BER performance in fading channel case when both IQ imbalance and PA non-linearity are compensated is shown in Fig. 9. The channel model used in the simulations is a non-line-of-sight indoor channel with 50 ns averaged root mean squared delay spread. The used model is available in the ADS software. With 10 dBm SI power, the performance of the FD link is the same as with HD link. With 20 dBm SI power, the performance difference between the HD and FD systems is about 1 dB which is the same difference than in the AWGN case[1].

7.5 Full-duplex link sum rate

As was seen in the Section 7.3, the noise level of a transceiver operating in the FD mode can be higher than that in the HD mode because of the imperfect SI cancelation. The

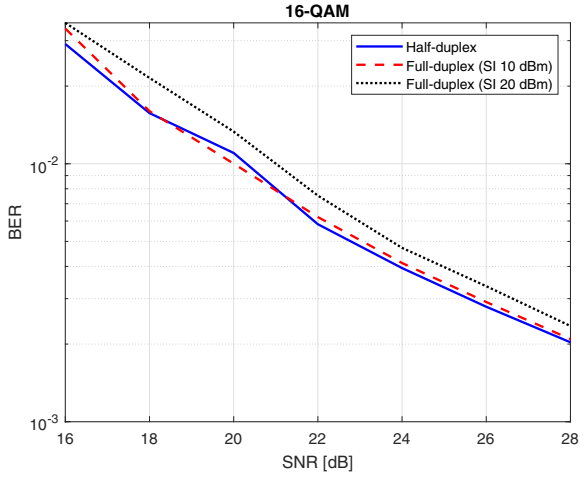

Fig. 9 BER vs. SNR in fading channel

effect of the increased noise level on the sum rate of a FD link can be evaluated with (25). Since both the RF cancelation and SI channel estimation are performed using the transmitted data signal in the HD mode, no additional FD specific pilots or training signals are used and hence $\kappa_{FD} = 0$. The data transmission between the nodes 1 and 2 requires the usage of pilots for the synchronization and channel estimation. Because the goal is to investigate the impact of the SI cancelation on the sum rate, the κ_{FD} is also set to zero here. It is further assumed that the transceivers at nodes 1 and 2 are identical and the performance of the SI cancelation at the both nodes is the same; hence, the SINR at the both nodes is assumed to be the same ($\gamma_1 = \gamma_2$).

The effect of residual SI on the sum rate is shown in Fig. 10. The horizontal axis gives the SNR in an ideal case, i.e., when the SI cancelation has removed all interference. The HD curve gives the sum rate on a HD link and the 0 dB curve shows the capacity of an ideal FD link (no residual SI). Curves labeled with 1 dB, 3 dB, 5 dB, 7 dB, and 10 dB show the capacity when the residual SI has decreased the SINR with 1 dB, 3 dB, 5 dB, 7 dB, and 10 dB, respectively. When the SINR reduction due to the residual SI is less than 5 dB, the FD link capacity is always the same or higher than the capacity of a HD link in an AWGN channel.

The effect of the tuning time of the RF canceler and the time needed for the SI estimation at the baseband unit on the spectral efficiency of the FD link is shown in Fig. 11. Curves labeled with $\beta = 0.9$ and $\beta = 0.6$ represent the cases where no data is received from the distant node during the tuning and SI channel estimation and they require 10% and 40% of the transmission time, respectively. Curves labeled with "$\beta = 0.9$ data" and "$\beta = 0.6$ data" are for the cases when tuning and SI channel estimation is done in the HD data transmission mode and they are needed during 10% and 40% of the transmission time, respectively. When the tuning of the RF canceler and SI channel estimation are needed seldom, the FD link capacity is not drastically decreased. On the other hand, when they are needed more frequently, their impact on the capacity increases. On the other hand, when they are performed while transmitting data in the HD mode, the effect of the tuning time on the link capacity is not as severe as in the case when the data transmission

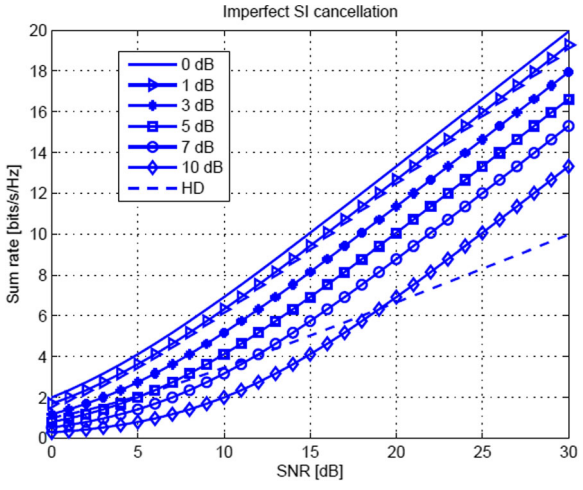

Fig. 10 FD link sum rate vs. SNR for different residual SI levels

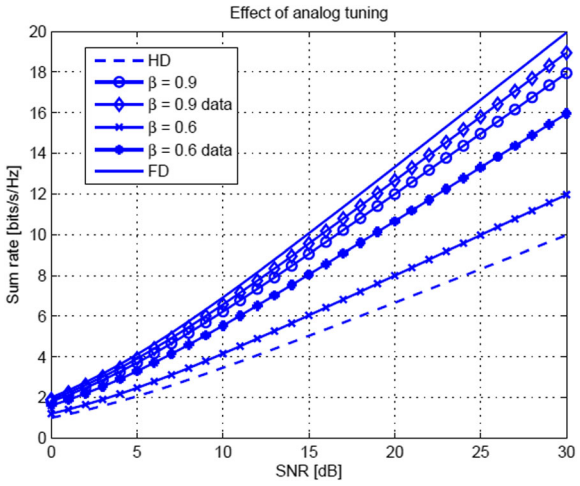

Fig. 11 FD link sum rate vs. SNR for different FD transmission/tuning time ratios

is stopped for the tuning, especially if the tuning and SI channel estimation needs to be done frequently.

The rate by which the tuning of the RF canceler and SI channel estimation needs to be done depends on the scenario and the assessment would require measurements. However, the results in [30] show that if there are reflective surfaces or objects near the FD transceiver, even a small movement, measured as a small fraction of the transmitted wave length, can cause drastic changes in the SI cancelation performance and hence necessitate re-tuning and estimation.

8 Discussion and conclusion

The effect of the SI cancelation on the FD link capacity was studied. A FD transceiver architecture, where SI cancelation is performed with three different techniques, (1) antenna isolation, (2) SI canceler operating at RF, and (3) digital SI cancelation at the baseband unit, was modeled. In order to have a realistic transceiver model, a simulation tool allowing to use the same format of component parameters that are used in the data sheets of commercial components was used to model the analog parts and A/D-converters of the FD transceiver. Baseband processing is modeled with Matlab. The ADS/Matlab co-simulation allowed also to control the RF canceler and the gain of the analog receiver chain.

Reflections from the environment decrease the isolation of the antenna but the usage of a RF canceler improves the total isolation at the RF. Depending on the SI channel realization, the RF canceler gives around 30 dB of additional cancelation as long as the largest delay of the RF canceler is not significantly shorter than the maximum delay of the SI channel. The performance is in the same order as the results in, e.g., [11, 14], although there are differences in the transceiver models and system setups and models. The RF canceler can be tuned and the SI channel can be estimated using the transmitted data signal for the training. Since the system can operate in the HD mode during the tuning, the sum rate of the link can be kept at a higher level than in the case, where the training and SI channel estimation would be done off-line. The non-linearity of a PA and IQ imbalance in the receiver is taken into account in the baseband SI cancelation. With low

transmit powers, the effect of the non-linearity and IQ imbalance are below the thermal noise power. When the transmit power is increased to 20 dBm, their effect without compensation is clearly visible. By using a simple iterative processing, their effect can be efficiently canceled. The remaining limiting factors in the baseband cancelation are the phase noise and IQ imbalance at the transmitter. If FD transmission is planned to be used in wireless systems with high transmit power, the transmitter IQ imbalance compensation should be included in the SI cancelation. The transmitter IQ balance compensation in non-linear SI channel is left for the future work. High transmit power can also drive the LNA into non-linear region. One topic for future work is to design a SI canceler that can take into account more than one non-linear component in the system. The transmitter and receiver chains were modeled as frequency flat circuits. In wideband systems, this assumption does not necessarily hold and the frequency response of the transmitter and receiver should be taken into account.

If the SI channel varies frequently, the capacity improvement by the FD transmission can be compromised, since the system must switch to the HD mode for the tuning of the RF canceler and baseband SI channel estimation. The variation in the SI channel can be smaller and slower in scenarios were the FD transmitter is static, i.e, access point/base station and in the cases where the frequency of the transmission is low. After the RF canceler has been tuned, the baseband SI channel estimation can be performed also in the FD mode [20, 27, 28]. This can increase the benefit of the FD transmission by increasing the throughput. However, the number of samples needed to estimate the SI channel in the HD mode is much lower than in the FD mode. Hence, the choice in this paper was to perform the SI channel estimation in the HD mode.

The joint modeling of analog SI cancelation at radio frequencies (both antenna and RF circuit based cancelers) using a software tool capable to model the behavior of real antennas and RF components and of baseband processing limits the possibility to do wider system level simulations. However, the results can be used to generate system level models where the performance of transceivers can be modeled with realistic parameters. But in order to gain understanding on the real benefits of FD transmission and on the other hand fully understand the restrictions on the performance, realistic simulation scenarios as well as test implementations are required in the future.

Abbreviations

A/D: Analog-to-digital; ADS: Advanced design system; AGC: Automatic gain control; AWGN: Additive Gaussian noise; BER: Bit error rate; D/A: Digital-to-analog; dB: Decibel; dBm: Decibel milliwatt; DNL: Differential non-linearity; FD: Full-duplex; FIR: Finite impulse response; HD: Half-duplex; I: In-phase; INL: Integral non-linearity; LO: Local oscillator; OFDM: Orthogonal frequency division multiplexing; PA: Power amplifier; Q: Quadrature-phase; QAM: Quadrature amplitude modulation; RF: Radio frequency; RX: Receiver; SINR: Signal to interference and noise ratio; SNR: Signal to noise ratio; SI: Self-interference; TCM: Theory of characteristic modes; TOI: Third-order intermodulation intercept point; TX: Transmitter

Acknowledgements

Not applicable.

Authors' contributions

Visa Tapio has developed the used methods and simulation models and performed all the simulations. Marko Sonkki has designed the antenna and prepared the S-parameter files used in the simulations. Markku Juntti has supervised the work and contributed to the writing of the article. The authors read and approved the final manuscript.

Funding

The research has been partially funded by Business Finland (formerly Tekes - the Finnish Funding Agency for Innovation), Nokia Oyj, Esju Oy, and CoreHW, and partially by the Academy of Finland 6Genesis Flagship (grant 318927).

Availability of data and materials

Not applicable.

Competing interests
The authors declare that they have no competing interests.

Author details
[1]Centre for Wirless Communications, University of Oulu, Oulu, Finland. [2]Present Address: Antenna Company, High Tech Campus 41, 5656 Eindhoven, AE, The Netherlands.

Received: 12 October 2019 Accepted: 21 May 2020
Published online: 18 June 2020

References

1. L. Anttila, D. Korpi, V. Syrjälä, M. Valkama, in *2013 Asilomar Conference on Signals, Systems and Computers*, Cancellation of power amplifier induced nonlinear self-interference in full-duplex transceivers, (2013). https://doi.org/10.1109/ACSSC.2013.6810482
2. J. I. Choi, M. Jain, K. Srinivasan, P. Levis, S. Katti, in *Proceedings of the Sixteenth Annual International Conference on Mobile Computing and Networking, MobiCom '10*, Achieving single channel, full duplex wireless communication (ACM, New York, 2010), pp. 1–12. http://doi.acm.org/10.1145/1859995.1859997
3. C. F. N. Cowan, Performance comparisons of finite linear adaptive filters. IEE Proc. F - Commun. Radar Sig. Proc. **134**(3), 211–216 (1987). https://doi.org/10.1049/ip-f-1:19870046
4. B. Debaillie, B.roek. van den D.J., C. Lavín, B. van Liempd, E. A. M. Klumperink, C. Palacios, J. Craninckx, B. Nauta, A. Pärssinen, Analog/RF solutions enabling compact full-duplex radios. IEEE J. Sel. Areas Commun. **32**(9), 1662–1673 (2014). https://doi.org/10.1109/JSAC.2014.2330171
5. L. Espenschied, High-frequency transmission system (1949). US Patent 2,467,299
6. R. Garbacz, R. Turpin, A generalized expansion for radiated and scattered fields. IEEE Trans. Antennas Propag. **19**(3), 348–358 (1971). https://doi.org/10.1109/TAP.1971.1139935
7. A. Goldsmith, *Wireless Communications*. (Cambridge University Press, 2005). https://doi.org/10.1017/CBO9780511841224
8. R. Harrington, J. Mautz, Theory of characteristic modes for conducting bodies. IEEE Trans. Antennas Propag. **19**(5), 622–628 (1971). https://doi.org/10.1109/TAP.1971.1139999
9. S. Haykin, *Adaptive filter theory, third edition edn*. (Prentice Hall Inc., 1996)
10. M. Heino, D. Korpi, T. Huusari, E. Antonio-Rodriguez, S. Venkatasubramanian, T. Riihonen, L. Anttila, C. Icheln, K. Haneda, R. Wichman, M. Valkama, Recent advances in antenna design and interference cancellation algorithms for in-band full duplex relays. IEEE Commun. Mag. **53**(5), 91–101 (2015). https://doi.org/10.1109/MCOM.2015.7105647
11. T. Huusari, Y. S. Choi, P. Liikkanen, D. Korpi, S. Talwar, M. Valkama, in *2015 IEEE 81st Vehicular Technology Conference (VTC Spring)*, Wideband self-adaptive RF cancellation circuit for full-duplex radio: operating principle and measurements, (2015). https://doi.org/10.1109/VTCSpring.2015.7146163
12. M. Jain, et al., in *Proceedings of the 17th Annual International Conference on Mobile Computing and Networking (MobiCom '11)*, Practical, real-time, full duplex wireless (ACM, New York, 2011), pp. 301–312. http://doi.acm.org/10.1145/2030613.2030647
13. A. Khandani, Methods for spatial multiplexing of wireless two-way channels (2010). US Patent 7 817 641
14. K. E. Kolodziej, J. G. McMichael, B. T. Perry, Multitap RF canceller for in-band full-duplex wireless communications. IEEE Trans. Wirel. Commun. **15**(6) (2016). https://doi.org/10.1109/TWC.2016.2539169
15. K. Komatsu, Y. Miyaji, H. Uehara, Basis function selection of frequency-domain Hammerstein self-interference canceller for in-band full-duplex wireless communications. IEEE Trans. Wirel. Commun. **17**(6), 3768–3780 (2018). https://doi.org/10.1109/TWC.2018.2816061
16. D. Korpi, L. Anttila, Syrjä V., M. Valkama, Widely linear digital self-interference cancellation in direct-conversion full-duplex transceiver. IEEE J. Sel. Areas Commun. **32**(9) (2014). https://doi.org/10.1109/JSAC.2014.2330093
17. D. Korpi, L. Anttila, M. Valkama, Nonlinear self-interference cancellation in MIMO full-duplex transceivers under crosstalk. EURASIP J. Wirel. Commun. Netw. **2017**(1), 24 (2017). https://doi.org/10.1186/s13638-017-0808-4
18. D. Korpi, Y. Choi, T. Huusari, L. Anttila, S. Talwar, M. Valkama, in *2015 IEEE Global Communications Conference (GLOBECOM)*, Adaptive nonlinear digital self-interference cancellation for mobile inband full-duplex radio: algorithms and RF measurements, (2015), pp. 1–7. https://doi.org/10.1109/GLOCOM.2015.7417188
19. E. H. Krishna, M. Raghuram, K. V. Madhav, K. A. Reddy, in *10th International Conference on Information Science, Signal Processing and their Applications (ISSPA 2010)*, Acoustic echo cancellation using a computationally efficient transform domain LMS adaptive filter, (2010), pp. 409–412. https://doi.org/10.1109/ISSPA.2010.5605458
20. A. Masmoudi, T. Le-Ngoc, Channel estimation and self-interference cancelation in full-duplex communication systems. IEEE Trans. Veh. Technol. **66**(1), 321–334 (2017). https://doi.org/10.1109/TVT.2016.2540538
21. MAX/2828/2829, Single-/dual-band 802.11 a/b/g world-Band transceiver ICs. Data sheet, Maxim Integrated Products, Inc. Available at https://datasheets.maximintegrated.com/en/ds/MAX2828-MAX2829.pdf
22. G. Panda, B. Mulgrew, C. Cowan, P. Grant, A self-orthogonalizing efficient block adaptive filter. IEEE Trans. Acoust. Speech. Sig. Proc. **34**(6), 1573–1582 (1986). https://doi.org/10.1109/TASSP.1986.1164996
23. A. Sethi, V. Tapio, M. Juntti, in *2014 IEEE Wireless Communications and Networking Conference (WCNC)*, Self-interference channel for full duplex transceivers, (2014). https://doi.org/10.1109/WCNC.2014.6952167
24. Reflection from the surface of the earth. Report 1008-1, International Telecommunication Union (ITU)
25. M. Sonkki, J. Aikio, M. Leinonen, A. Pärssinen, Study of transmitter interference to receiver at 2 GHz with high antenna port isolation. Prog. Electromagn. Res. M. **86**, 183–192 (2019)
26. V. Tapio, H. Alves, M. Juntti, in *2017 IEEE International Conference on Acoustics, Speech and Signal Processing (ICASSP)*, Joint analog and digital self-interference cancellation and full-duplex system performance, (2017), pp. 6553–6557. https://doi.org/10.1109/ICASSP.2017.7953419
27. V. Tapio, M. Juntti, A. Pärssinen, K. Rikkinen, in *2016 50th Asilomar Conference on Signals, Systems and Computers*, Real time adaptive RF and digital self-interference cancellation for full-duplex transceivers, (2016), pp. 1558–1562. https://doi.org/10.1109/ACSSC.2016.7869640

28. V. Tapio, M. Sonkki, in *22th European Wireless Conference European Wireless 2016*, Analog and digital self-interference cancellation for full-duplex transceivers, (2016), pp. 1–5
29. V. Tapio, M. Sonkki, M. Juntti, in *2018 IEEE 87st Vehicular Technology Conference (VTC Spring)*, Analog self-interference cancellation with automatic gain control for full-duplex transceivers, (Porto, 2018). https://doi.org/10.1109/VTCSpring.2018.8417518
30. V. Tapio, M. Sonkki, M. Juntti, in *2018 IEEE 29th Annual International Symposium on Personal, Indoor and Mobile Radio Communications (PIMRC)*, Performance of a full-duplex system in non-linear and time-varying self-interference channel, (Bologna, 2018). https://doi.org/10.1109/PIMRC.2018.8580927
31. A. Tarighat, A. H. Sayed, in *2004 IEEE International Conference on Acoustics, Speech, and Signal Processing, vol. 4*, On the baseband compensation of IQ imbalances in OFDM systems, (2004). https://doi.org/10.1109/ICASSP.2004.1327003
32. K. Wang, R. Zhang, Z. Zhong, X. Zhang, X. Pang, in *2017 IEEE International Conference on Communications Workshops (ICC Workshops)*, Measurement of self-interference channels for full-duplex relay in an urban scenario, (2017), pp. 1153–1158. https://doi.org/10.1109/ICCW.2017.7962814
33. T. Warnagiris, An alternative full-duplex transceiver architecture based on spatially distributed oscillators. RF Des. **20**(7), 32–43 (1997)
34. Z. Zhang, X. Chai, K. Long, A. V. Vasilakos, L. Hanzo, Full duplex techniques for 5g networks: self-interference cancellation, protocol design, and relay selection. IEEE Commun. Mag. **53**(5), 128–137 (2015). https://doi.org/10.1109/MCOM.2015.7105651
35. G. T. Zhou, H. Qian, L. Ding, R. Raich, On the baseband representation of a bandpass nonlinearity. IEEE Trans. Sig. Proc. **53**(8), 2953–2957 (2005). https://doi.org/10.1109/TSP.2005.850383

Publisher's Note